Title

Anatomy of an agricultural antagonist: Feeding complex structure and function of three xylem sap-feeding insects illuminated with synchrotron-based 3D imaging

Journal

Journal of Morphology, 284(10)

ISSN

0362-2525

Authors

Clark, Elizabeth G

Cornara, Daniele

Brodersen, Craig R

et al.

Publication Date

2023-10-01

DOI

10.1002/jmor.21639

Received: 8 June 2023 | Revised: 14 August 2023 | Accepted: 20 August 2023

DOI: 10.1002/jmor.21639

RESEARCH ARTICLE

JOURNAL OF morphology WILEY

Anatomy of an agricultural antagonist: Feeding complex structure and function of three xylem sap-feeding insects illuminated with synchrotron-based 3D imaging

Elizabeth G. Clark[1] | Daniele Cornara[2] | Craig R. Brodersen[3] | Andrew J. McElrone[4] | Dilworth Y. Parkinson[5] | Rodrigo P. P. Almeida[1]

[1]Department of Environmental Science, Policy and Management, University of California Berkeley, Berkeley, California, USA

[2]Department of Soil, Plant, and Food Sciences (DiSSPA), University of Bari, Bari, Italy

[3]School of the Environment, Yale University, New Haven, Connecticut, USA

[4]USDA Agricultural Research Service, Davis, California, USA

[5]Advanced Light Source, Lawrence Berkeley National Laboratory, Berkeley, California, USA

Correspondence
Rodrigo P. P. Almeida and Elizabeth G. Clark, Department of Environmental Science, Policy and Management, University of California Berkeley, Berkeley, CA 94720, USA.
Email: rodrigoalmeida@berkeley.edu and elizabethclark@berkeley.edu

Funding information
US Department of Energy; California Department of Food and Agriculture PD/GWSS Research Program, Grant/Award Number: 21-0274-000-SA; Marie Skłodowska-Curie, Grant/Award Number: 835732 XYL-SPIT

Abstract

Many insects feed on xylem or phloem sap of vascular plants. Although physical damage to the plant is minimal, the process of insect feeding can transmit lethal viruses and bacterial pathogens. Disparities between insect-mediated pathogen transmission efficiency have been identified among xylem sap-feeding insects; however, the mechanistic drivers of these trends are unclear. Identifying and understanding the structural factors and associated integrated functional components that may ultimately determine these disparities are critical for managing plant diseases. Here, we applied synchrotron-based X-ray microcomputed tomography to digitally reconstruct the morphology of three xylem sap-feeding insect vectors of plant pathogens: *Graphocephala atropunctata* (blue-green sharpshooter; Hemiptera, Cicadellidae) and *Homalodisca vitripennis* (glassy-winged sharpshooter; Hemiptera, Cicadellidae), and the spittlebug *Philaenus spumarius* (meadow spittlebug; Hemiptera, Aphrophoridae). The application of this technique revealed previously undescribed anatomical features of these organisms, such as key components of the salivary complex. The visualization of the 3D structure of the precibarial valve led to new insights into the mechanism of how this structure functions. Morphological disparities with functional implications between taxa were highlighted as well, including the morphology and volume of the cibarial dilator musculature responsible for extracting xylem sap, which has implications for force application capabilities. These morphological insights will be used to target analyses illuminating functional differences in feeding behavior.

KEYWORDS

3D imaging, Auchenorryncha, functional morphology, vectors of plant pathogens, xylem sap-feeding insects

1 | INTRODUCTION

Insects within the suborder Auchennoryncha such as sharpshooter leafhoppers, spittlebugs, and cicadas feed on the xylem sap of plants. Several distinctive challenges are associated with this lifestyle. While phloem is rich in sugar and amino acids, xylem sap is nutritionally poor; as such, these insects must extract a large amount of fluid from the plants to meet their metabolic needs (Raven, 1983). It has been estimated that daily rates of ingestion may reach 1000 times the mass of the insect (Mittler, 1967) and that the rate of fluid flow through their mouthparts likely surpasses 1 m/s (Ranieri et al., 2020). Furthermore, xylem sap is energy intensive to extract: while phloem is under positive pressure and can be extracted passively, xylem sap is under negative pressure (i.e., tension), and extraction requires the application of large amounts of force to overcome the pressure differential between the plant and insect (Bergman et al., 2021; Raven, 1983). Many questions remain unanswered regarding this unusual feeding strategy, such as how xylem sap-feeding insects generate the forces necessary to overcome the extreme negative pressures of the xylem vessels and how they are able to sustain such a large daily fluid intake. Understanding xylem sap ingestion in these insects is of applied relevance because they can transmit the xylem-limited bacterial plant pathogen *Xylella fastidiosa* over the course of feeding (Sicard et al., 2018). The threat of *X. fastidiosa* to agriculture continues to increase globally, and without curative methods available to limit disease impacts, further investigation to better understand the biology of this system is necessary.

Xylem sap-feeding insects are nested within the monophyletic suborder Auchenorryncha (Cryan & Urban, 2012) within the order Hemiptera; the suborder includes members of the Aphrophoridae (superfamily Cercopoidea, spittlebugs and froghoppers) and Cicadidae (cicadas) as well as members of the Cicadellidae (leafhoppers; Cryan & Urban, 2012). The most notable vector of *X. fastidiosa* in the United States has historically been the leafhopper *Graphocephala atropunctata* (Cicadellidae: Cicadellinae) (Tumber et al., 2014); however, the spread of diseases caused by *X. fastidiosa* in California have increased following the introduction of an invasive leafhopper, *Homalodisca vitripennis* (Cicadellidae: Cicadellinae) (Redak et al., 2004; Tumber et al., 2014). The meadow spittlebug *Philaenus spumarius* (Cercopoidea: Aphrophoridae) is an important insect vector of *X. fastidiosa* in Europe (Cornara et al., 2019) and is also present in California, along with *G. atropunctata* and *H. vitripennis*. Collectively, they represent a diverse set of insects that have all evolved to feed on xylem sap, which presents an opportunity for exploring the functional similarities across xylem sap-feeding taxa.

Differences in transmission efficiency among these *X. fastidiosa* vectors have been known for some time. For example, in grapevines, *G. atropunctata* is more efficient than *H. vitripennis* in transmitting *X. fastidiosa* (Almeida & Purcell, 2003; Daugherty & Almeida, 2009; Purcell, 1979; Purcell & Saunders, 1999). Disparate anatomy and relative sizes of components of the feeding complex between taxa may have a role in these differential transmission rates. The structure of the functional foreguts of xylem sap-feeding insects have been examined through dissection with traditional microscopy, scanning electron microscopy (SEM), and microcomputed tomographic (micro-CT) imaging (Backus et al., 2012, Backus & McLean, 1982; Bergman et al., 2021; Killiny & Brodersen, 2022; Leopold et al., 2003; Ranieri et al., 2020; Ruschioni et al., 2019; White et al., 2021). However, a high-resolution comparative examination of the 3D structure between species remains to be conducted and represents a necessary step toward understanding the physiology of ingestion and bacterial transmission. Here, through the application of synchrotron-based X-ray micro-CT imaging, we generated 3D images and digital reconstructions of key internal features of the feeding complex of xylem sap-feeding insects *G. atropunctata*, *H. vitripennis*, and *P. spumarius*, including the cibarial dilator musculature, the food canal, the precibarial valve, and salivary organs. The application of this technique revealed new anatomical details critical to illuminate aspects of the process of xylem sap ingestion and highlighted important differences between taxa with functional implications.

1.1 | General anatomy of the feeding complex

Xylem sap-feeding insects have a specialized feeding complex to aid in sap extraction and ingestion. These three insect species have a homologous suite of components within the head integrated to form the feeding complex (Figure 1): the stylets and food canal, the precibarium and the precibarial canal, the cibarium, the salivary organs, and their associated musculature. The distalmost part of the feeding apparatus is made of interlocking maxillary stylets forming the food and salivary canals, which are surrounded by two mandibular stylets (stylet fascicle; Backus, 1985; Figure 2, Supporting Information: Figures S1, S2). The interlocking portion is positioned within the crease of the three segmented labium. The labrum is a segment adjacent to the labium and stylet fascicle, approaching a cone-like shape. To initiate feeding, the insect inserts these modified mouthparts into the plant. Next, movement of the stylets within the plant allows the insect to probe for a suitable xylem vessel.

The hypopharynx and the epipharynx are fused to form the precibarium, which houses the precibarial valve and precibarial canal (Backus & McLean, 1982; Ruschioni et al., 2019). Near the proximal interlocking juncture of the stylets, a hypopharyngeal extension (Almeida & Purcell, 2006) connects the precibarium and the food canal so that the fluid within the food canal flows into the precibarial canal, with a ~120° angle formed at this juncture. The cibarium (Figure 2) is a chamber connecting the precibarium and the esophagus (Nault & Ammar, 1989). Contraction of the cibarial dilator muscles creates negative pressure, which pulls fluid into the cibarium; the collapse of the cibarial diaphragm following muscular relaxation pushes the fluid in the cibarium through the esophageal valve toward the esophagus and into the midgut. Here, we report several new anatomical features revealed through this 3D digital visualization of the feeding complex.

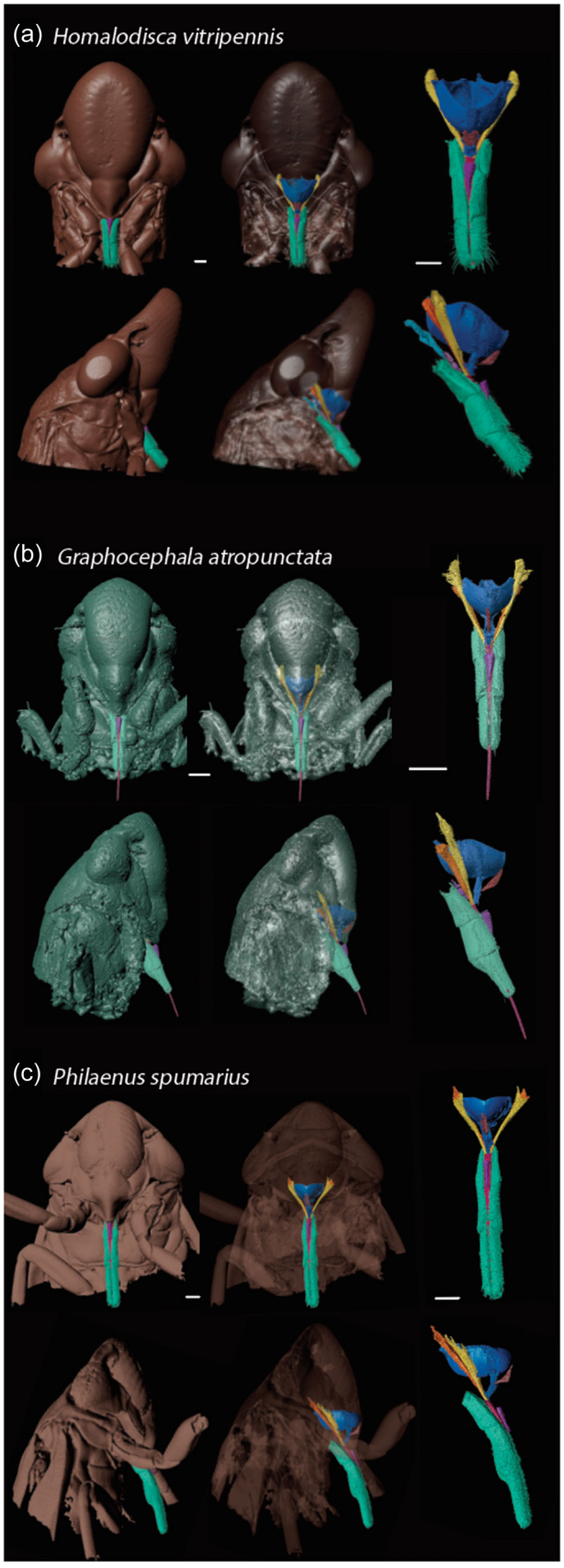

1.2 | Functional anatomy of the precibarium and precibarial valve

Although the rate of fluid flow is dictated mainly by the rate and degree of contraction of the cibarial pump, the direction of fluid flow is controlled in the insect by a few physical mechanisms: the precibarial valve and the esophageal valve. These valves are located on either side of the cibarial pump: the esophageal valve is located proximally and the precibarial valve on the distal end. The precibarial valve bisects the length of the precibarial canal and controls the flow of fluid from the food canal within the stylets into the cibarium (Backus & McLean, 1982). The esophageal valve is a passive one-way valve that permits flow of fluid from the cibarium to the esophagus/midgut and prevents reversal of flow (Ruschioni et al., 2019). However, the precibarial valve is actively controlled by the contraction of precibarial valve musculature. Therefore, the closing mechanism of the valve within the precibarium has critical implications for the flow of fluid in this system. Furthermore, colonization of bacteria within the precibarium has been found to correlate with successful transmission of *X. fastidiosa* during feeding (Almeida & Purcell, 2006). As such, understanding the mechanistic role of the precibarium and the precibarial valve in fluid flow is therefore critical to illuminating the transmission dynamics of this pathogen.

The dynamics of fluid flow about the precibarial valve remain understudied, and a full high-resolution 3D visualization of the anatomy is necessary to understand this process. It has been unclear if the precibarial valve fully closes. This has critical implications for the dynamics of fluid flow within the feeding canal, as the precibarial valve is proximal to the point at which the canal interfaces with the atmosphere and the xylem vessel. If the flap within the precibarial valve cannot fully seal the end of the canal from the rest of the system, fluid could continuously flow from the proximal areas of the canal, such as the cibarium, into the food canal of the stylet fascicle. This could, for example, cause fluid to leak from the tip of the stylets and allow air to enter the cibarium after extraction from the xylem vessel. However, if the precibarial valve flap completely seals off these two areas, it would limit backflow from the proximal precibarial canal and keep the liquid inside the canal proximal to the precibarial valve under tension when the stylets are extracted from the xylem vessel. We used our 3D imaging data to determine whether or not the precibarial valve fully closes.

FIGURE 1 3D structure of the head of (a) *Homalodisca vitripennis*, (b) *Graphocephala atropunctata*, and (c) *Philaenus spumarius* generated through synchrotron-based micro-CT imaging in frontal (top) and lateral (bottom) views. Includes the internal structure of the feeding complex (rightmost column in a, b, and c). Scale bars are 0.25 mm.

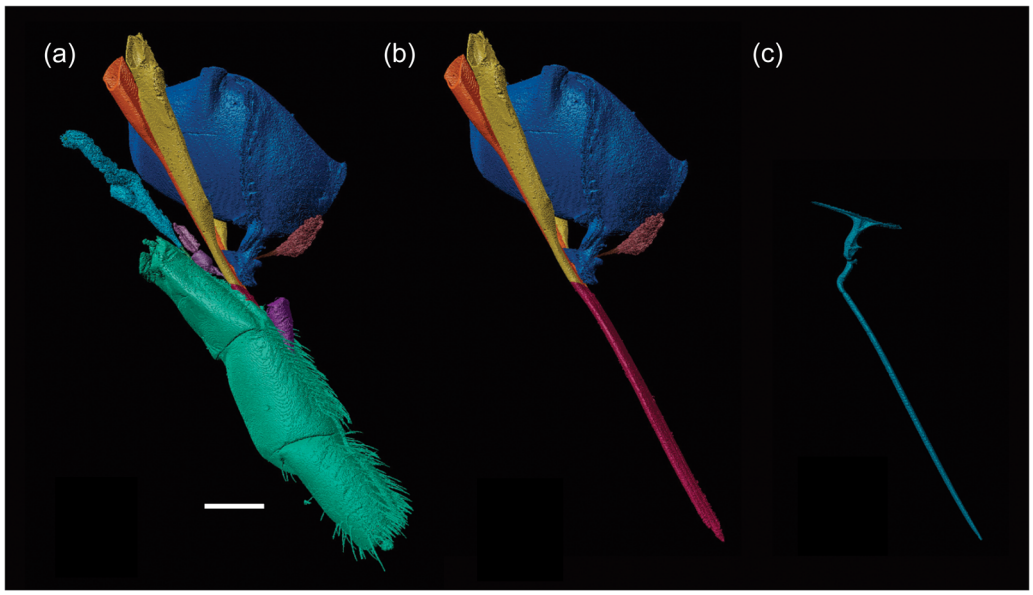

FIGURE 2 (a) Lateral view of the 3D structure of the feeding complex of *Homalodisca vitripennis*, including the labium (green), labrum (purple), cibarium (blue), maxillary stylets (orange), mandibular stylets (yellow), and precibarial valve muscle (red), and the distal end of the stylet fascicle (pink). (b) Labium and labrum removed, revealing the stylet fascicle and the juncture with the proximal portions of the mandibular stylets and maxillary stylets. (c) Internal volume of the canal within the cibarium and stylet fascicle. Scale bar is 0.25 mm.

Furthermore, the mechanism of closure of the precibarial valve has been debated. The precibarial valve of leafhoppers was first described in Backus and McLean (1982) as a unit of cuticle located half-way along the precibarium. The base of this unit (subsequently described elsewhere as the "flap") was attached to the proximal edge of a "pit," and the pit was described as being connected to the apodeme of the precibarial valve muscle (see Figure 2 of Backus & McLean, 1982). The mechanism for valve closure suggested was that when the muscle contracts, the flap hinges downward (i.e., the far end of the valve swings toward the hypopharynx), effectively closing the food canal (Backus & McLean, 1982). Ruschioni et al. (2019) provided a disparate interpretation of the anatomy of the precibarial valve with consequences for its underlying function. In contrast to Backus and McLean (1982), a larger portion of the precibarium was considered to work as the valve in addition to the cuticular flap. The cuticular flap, as in Backus and McLean (1982), is described as articulating with the edge of the pit; however, here the rim of the pit is referred to as the "ring" and the pit itself is called the "bell-like invagination." The precibarial valve muscle is called the "basin-like muscle," and the muscle was interpreted to attach to a "basin-like structure" that sits proximally to the flap along the epipharynx (see Figure 3 in Ruschioni et al., 2019). This is notably in contrast to the Backus and McLean (1982) interpretation, where this muscle was attached to the bell-like invagination (i.e., the pit). In the Ruschioni et al. (2019) model, contraction of the basin-like muscle would pull the cuticle of the basin-like structure, which would pull the flap away from the hypopharynx (effectively opening the food canal). Closure of the flap was hypothesized to occur through a two-pronged mechanism: the relaxation of the muscle

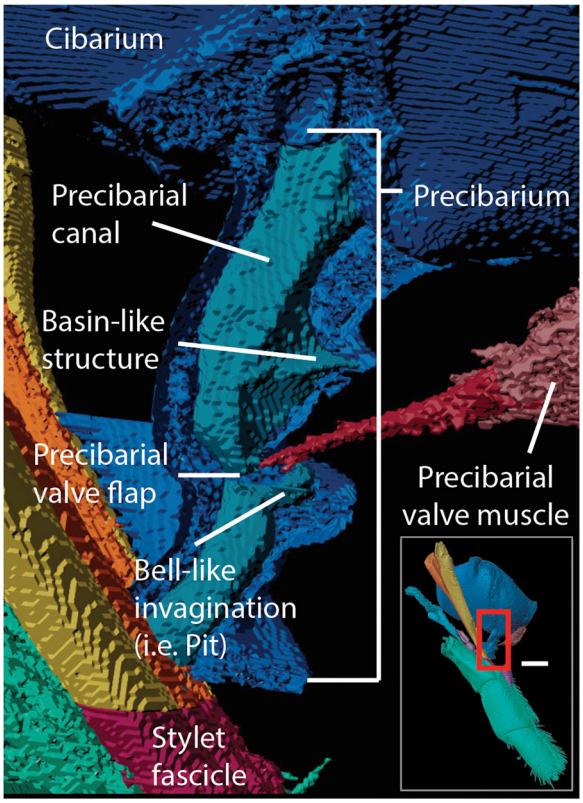

FIGURE 3 Lower right: Lateral view of the feeding complex of *Homalodisca vitripennis* from Figure 2 with scale bar of 0.25 mm. Red box indicates enlarged area to left. Cuticular area of precibarium (dark blue) bisected to reveal the internal cavity of the precibarial canal (light blue).

would move the flap toward the hypopharynx resulting in partial valve closure. Fluid moving through the canal would then be funneled through the open ring toward the bell-like invagination which inflates to push the valve closed. Here, we collected 3D imaging data to observe the anatomy of the musculature associated with the precibarium to evaluate these hypotheses regarding the mechanics of function of the precibarial valve.

2 | MATERIALS AND METHODS

2.1 | Specimen acquisition

2.1.1 | *Graphocephala atropunctata* (Signoret, 1854)

Specimens were reared to the adult stage from eggs laid in captivity by the in-house colony of *G. atropunctata* maintained at the Oxford Tract Facility at UC Berkeley. Specimens were kept in shaded mesh cages (Bug Dorm-2®; BioQuip Products) with approximately 500–1000 individuals per cage. The insects were reared on 1-month old basil (*Ocimum basilicum* L. cv. Genovese) plants, grown in 3 L pots filled with Sunshine Mix #4 (Sungro Horticulture). These plants were replaced every 2 weeks and watered every other day inside an insect-proof greenhouse at 24°C constant, 60% HR, and photoperiod 12:12L:D.

2.1.2 | *Philaenus spumarius* (Linnaeus, 1758)

A colony of *P. spumarius* was started from third to fourth instar nymphs collected in Berkeley and San Francisco on *Euphorbia* spp. and fennel (*Foeniculum vulgaris*), and reared on grapevine (*Vitis vinifera*), vetch (*Vicia sativa*), sunflower (*Helianthus annuus*), fava bean (*Vicia faba*), and *Sonchus* sp. until adulthood inside shaded Bug Dorm mesh tents (approx. 500 nymphs per cage). Once emerged, adults were reared on grapevine and sunflower in Bugdorms (approx. 400 adults per cage) grown inside a greenhouse shaded with a shading net at controlled conditions (24–18°C [day-night], photoperiod 14:10L:D, 60% HR), with the plants water-fertilized three times per week and replaced once a month.

2.1.3 | *Homalodisca vitripennis* (Germar, 1821)

Specimens were collected as eggs in Bakersfield, during the spring of 2020 and transported to a laboratory at the USDA-ARS San Joaquin Valley Agricultural Sciences Center in Parlier. Groups of about 100 nymphs were reared to the adult stage in mesh cages (Bug Dorm-2®; BioQuip Products) containing four plant species: cowpea (*Vigna unguiculata* L. Walp. cv. Blackeye), okra (*Abelmoschus esculentus* [L.] Moench cv. Cajun delight), basil (*O. basilicum* L. cv. Genovese), and sunflower (*H. annuus* L. cv. American Giant Hybrid; see Krugner & Gordon, 2018).

2.2 | X-ray micro-CT imaging and data analyses

The specimens were scanned at beamline 8.3.2 of the Advanced Light Source at the Lawrence Berkeley National Laboratory. X-ray images were generated over the course of two to five scans for each specimen using a 4x objective lens. Four specimens of *G. atropunctata*, four specimens of *H. vitripennis*, and two specimens of *P. spumarius* were scanned, reconstructed (Gürsoy et al., 2014), and measured. Specimens were prepared for scanning using the protocol outlined in Wood and Parkinson (2019). They were stored in 70% ethanol, stained overnight before scanning in Lugol's solution, and washed in 70% EtOH for 30 min. Specimens were then placed within a pipette tip containing 70% EtOH for scanning. The pipette tip was affixed to a wooden rod and sealed on either end with epoxy. ~1750 unique images were generated for each specimen respectively and used to form reconstructed 3D images with a voxel size of 1.605 µm. The digital volume was visualized using Avizo Lite v. 9.2.0 (Thermo Fisher Scientific) and Dragonfly version 2021.3 (Object Research Systems), and a semiautomated volume thresholding tool was used to demarcate different anatomical features. Two dimensional measurements were performed in Dragonfly using the measurement tool. Volume was calculated using a region of interest demarcation tool in Dragonfly in which voxels were selected based on a threshold of greyscale values (which is an indication of relative density). The cibarial dilator muscles and the large, continuous cavity within the stylet fascicle (i.e., the food canal) and precibarium (i.e., the precibarial canal) were selected using this tool to measure the volume of these regions. As each voxel is a cube with a known edge length (in this case, 1.605 µm), the volume value given by Dragonfly represents the sum of the area of the voxels selected. The volumes of interest were each converted to a mesh and exported separately as a stereolithography 3D object file (STL). Meshlab (Cignoni et al., 2008) was used to remove external voxels, simplify larger meshes, and convert the files to wavefront (OBJ) (Clark et al., 2023). The meshes were then visualized and imaged using Maya (Autodesk).

3 | RESULTS

3.1 | The precibarium and precibarial valve

In all specimens examined, the cuticular precibarial valve flap is down, completely blocking the canal within the valve so that the fluid in the distal and proximal portions of the precibarium are separated (Figure 3 and Supporting Information: Figures S3, S4). The precibarial valve muscle is attached to the proximal portion of a pit near the base of the cuticular flap (Figure 3 and Supporting Information: Figures S3, S4).

3.2 | The cibarium and the cibarial dilator muscles

In each insect examined, we found that these units consist of approximately 30 separate fan-shaped muscles arranged in a

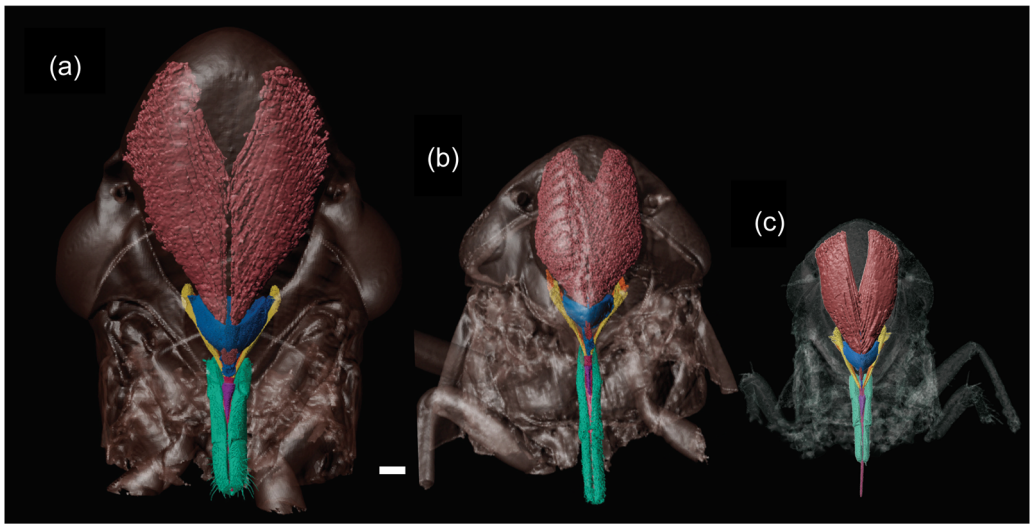

FIGURE 4 Front view of *Homalodisca vitripennis* (a), *Philaenus spumarius* (b), and *Graphocephala atropunctata* (c) revealing the structure of the cibarial dilator muscles in pink. External anatomy of the insect is at 90% transparency. Data represents a 3D reconstruction generated from micro-CT data. Scale bar is 0.25 mm. micro-CT, microcomputed tomographic.

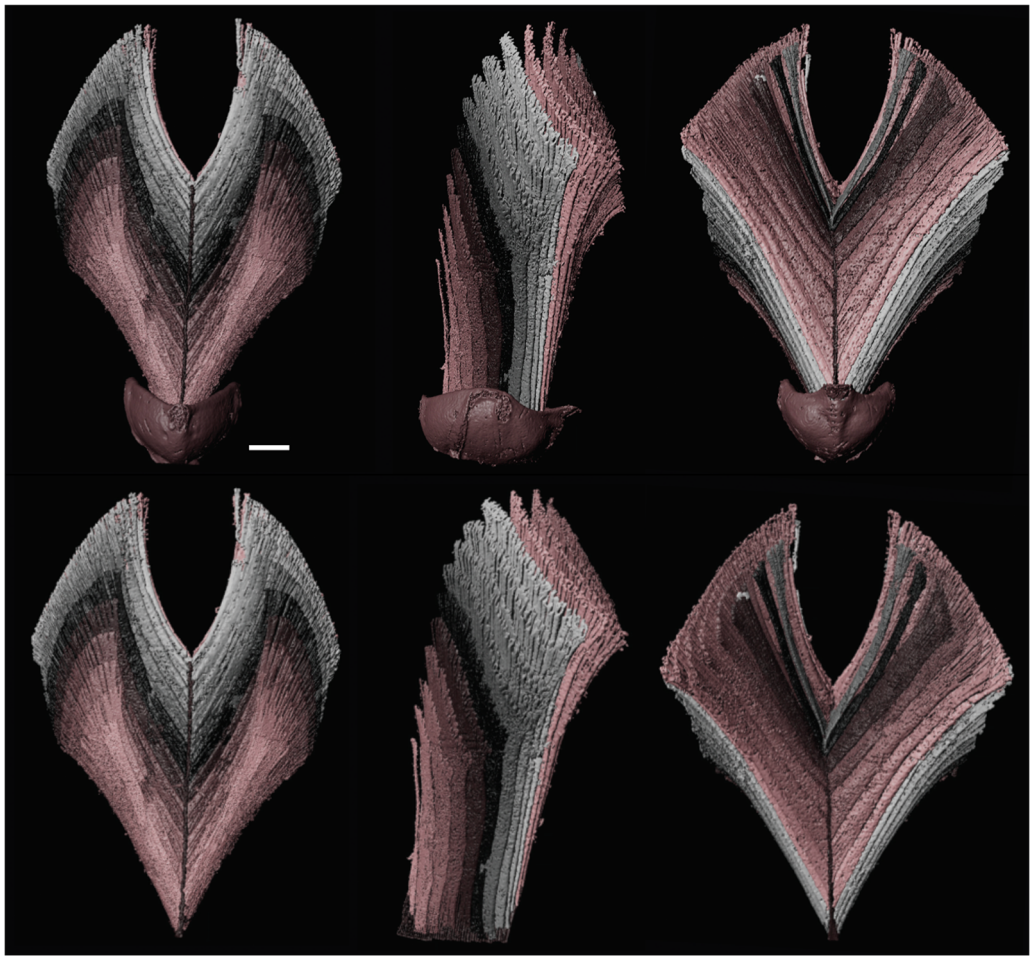

FIGURE 5 The cibarial dilator muscle unit in front (left), lateral (middle), and posterior (right) view, with and without the cibarium (above and below, respectively). Central apodeme bisects the two muscle units. Color gradient used to show 30+ individual muscle units with independent apodeme attachment sites. Scale bar is 0.25 mm.

bipinnate structure (Figures 4 and 5) that have an apodeme connected along the long axis of the cibarium representing the direction of force application. The opposing end of each muscle is attached to the inside of the head exoskeleton.

3.3 | The salivary complex

Xylem sap-feeding insects rely on an internal salivary complex to produce and deliver saliva through the stylets. The stylet fascicle contains a salivary canal at the dorsal boundary between the interlocking maxillary stylets. At the juncture where the stylets diverge, the anterior salivary duct (ASD) connects the salivary canal within the stylet fascicle to the salivarium (Figure 6). The salivarium has two structures connected to the proximal end: a reservoir ventrally and a common salivary duct (CSD) dorsally. The reservoir is attached to a v-shaped bipinnate muscle unit (Supporting Information: Figure S5). The internal tubing (lumen) of the CSD is surrounded by wall cells (Supporting Information: Figure S6). The CSD diverges in two away from the base into the efferent salivary duct (ESD) and wraps sinusoidally before diverging laterally from the base. Terminology to describe the morphology of the salivary complex was adapted from Wang et al. (2021).

3.4 | Interspecific disparities in scaling

The dimensions of the food canal and the precibarial canal vary among species due to the notable size differences between these insects (Table 1). For instance, the food canal in *G. atropunctata*, on average, was around half the size and volume of that in *H. vitripennis*. Furthermore, we found striking differences in the size of the muscles between the specimens of the different species examined here. The length of the cibarial dilator musculature of *H. vitripennis* was approximately 150% that of *G. atropunctata*, and the muscle volume of *H. vitripennis* was almost an order of magnitude larger than that of *G. atropunctata* (with an average of 1.54 mm^3 in *H. vitripennis*, 0.42 mm^3 in *P. spumarius*, and 0.16 mm^3 in *G. atropunctata*, see Table 1 and Supporting Information: Table S1).

4 | DISCUSSION

4.1 | The precibarium and the precibarial valve

The 3D images generated here allowed us to observe that the flap within the precibarial valve completely closes in each taxon, effectively sealing the distal precibarial canal off from the rest of the system (Figures 2 and 4). This would prevent fluid backflow and air transmission within the canal, which would improve feeding efficiency (Figure 7). The data also indicate that the precibarial valve is closed when the precibarial valve muscle is relaxed. We used this high-resolution visualization of the 3D morphology to evaluate hypotheses related to the mechanism of valve closure that have been proposed. Our 3D imaging data in all three insect taxa examined show that the muscle is not attached to the basin-like structure (Figure 3 and Supporting Information: Figures S3, S4). It is attached to the cuticle of the epipharynx at the proximal end of the ring by the base of the flap. As such, contraction of the "basin-like muscle" would not pull the basin-like structure to open the valve as suggested by Ruschioni et al. (2019). Instead, contraction of the muscle would pull the epipharynx directly at the point of attachment (at the base of the flap, i.e., the ring) to open the valve. Furthermore, given the revision

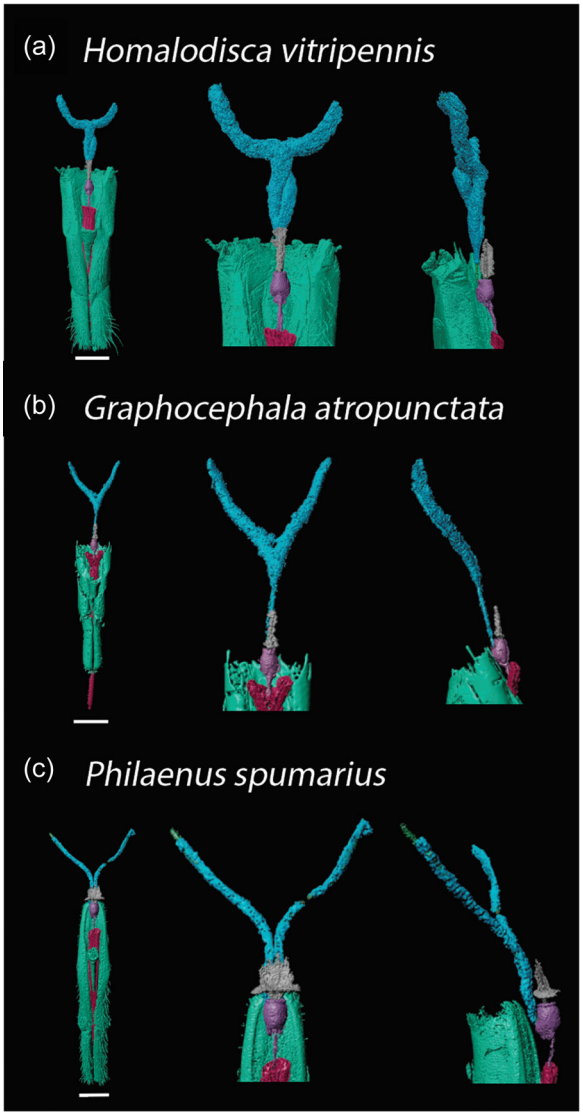

FIGURE 6 Front view (left), closeup front (middle), and lateral view (right) of the organs of the salivary system of *Homalodisca vitripennis* (a), *Graphocephala atropunctata* (b), and *Philaenus spumarius* (c) along with the stylet fascicle (pink), labium, and labrum (green). The anterior salivary duct is connected to the proximal end of the salivarium (purple). The salivarium is connected at the distal end to the reservoir (gray) and the common salivary duct (light blue). Scale bar is 0.25 mm. Terminology used to describe the morphology of the salivary complex was adapted from Wang et al. (2021).

TABLE 1 Average measurements of the feeding complex across specimens examined in this study.

Feature	*Homalodisca vitripennis*	*Philaenus spumarius*	*Graphocephala atropunctata*
Cibarium length (mm)	0.86	0.65	0.46
Cibarium width (mm)	0.61	0.43	0.32
Cibarium height (mm)	0.43	0.27	0.21
Precibarial canal length (mm)	0.24	0.25	0.17
Precibarial canal volume (mm^3)	0.0002	0.0001	0.00004
Food canal length (mm)	1.02	1.23	0.81
Food canal width (midpoint) (um)	20.31	17.05	11.95
Food canal volume mm^3	0.0003	0.0002	0.0001
Total cibarial dilator muscle height (mm)	2.40	1.41	1.08
Total cibarial dilator muscle length (mm)	0.82	0.62	0.41
Total cibarial dilator muscle width (mm)	1.58	0.92	0.67
Total cibarial dilator muscle volume mm^3	1.54	0.42	0.16

Note: Specimens measured in Dragonfly version 2021.3 (Object Research Systems).

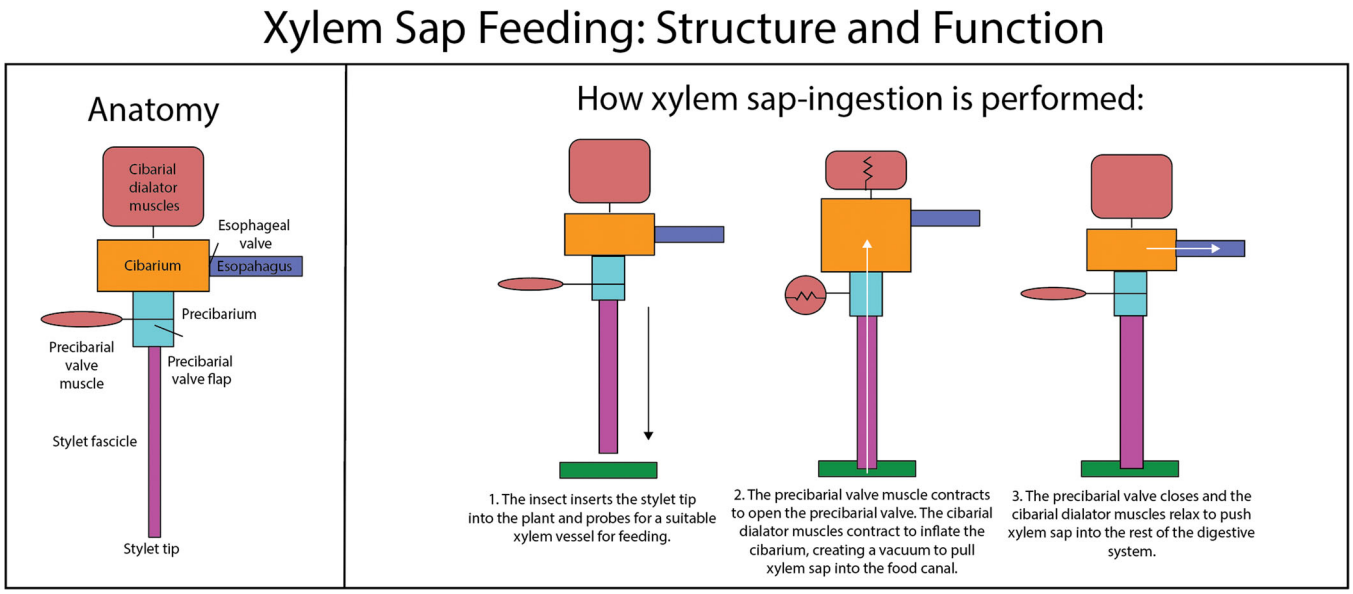

FIGURE 7 Simplified schematic of the anatomy of the feeding complex (left) and a diagram indicating how the different parts of the feeding complex function to facilitate ingestion (right). The 3D imaging results show that the precibarial valve is capable of full closure, which would seal the distal precibarial canal and food canal off from the rest of the system. This would facilitate feeding efficiency and may have implications for the dynamics of bacterial transmission. The precibarial valve muscle is attached at the base of the flap, so that contraction of this muscle would pull the valve open.

to the position of the muscle attachment and our observation of full valve closure, we can infer that movement of liquid into the bell-like invagination may not be necessary to fully close the food canal as proposed by Ruschioni et al. (2019). However, we hypothesize that the bell-like invagination and basin-like structure may still have a role in feeding. These areas, for instance, may enable recirculation of fluid moving toward the valve when it is closed. Our 3D imaging data reveals the morphology of the closed valve; as such, the specific angles of the flap in relation to the hypopharynx during feeding in vivo remain to be determined. High resolution imaging data from different sap ingestion stages will be necessary to address some of these questions.

4.2 | The cibarium and the cibarial dilator muscles

The cibarial dilator muscles consist of two bipinnate units symmetric across the central apodeme (Chapman, 1998; Snodgrass, 1935). The

muscles on the proximal membrane of the cibarium have been previously described as a two-unit muscle system (Chapman, 1998; Snodgrass, 1935). We found that these units are each comprised of a series of ~15 separate fan-shaped muscles (Figures 4 and 5). As the insects would be able to control the contraction of these muscles independently, instead of as a single unit, this would theoretically provide an exponentially higher number of possible coordination patterns to achieve different degrees of cibarial inflation, both in terms of total volume and the spatial distribution of the fluid. This would permit increased control over the rate and volume of fluid flow through the feeding complex. It is also possible that this may provide a level of redundancy in case of damage. This multi-muscle control scheme suggests that the nature of cibarial inflation is more dynamic than under a two-muscle system, and further in vivo study of cibarial contraction rates, fluid flow, muscle physiology, and cibarial pumping mechanics are necessary to understand the implications of the morphological disparities identified here.

4.3 | The salivary complex

The salivary organs remain poorly studied for this group of insects. We identified a number of organs in the distal salivary production complex, including the ASD, the salivarium, the CSD, reservoir, ESD, lumen, and wall cells (Figure 6 and Supporting Information: Figures S5, S6). The overall structure of the organs and their arrangement are similar to that in *Nilaparvata lugens*, a phloem sap-feeding planthopper in which these structures have also been digitally reconstructed in 3D (Wang et al., 2021). Saliva is produced in glands upstream and is transported through two salivary ducts. These merge to form a CSD, which is connected to a cup-shaped vessel known as the salivarium. A reservoir is connected to the proximal end of the salivarium. Dilator muscles (i.e., dilator of the salivary syringe) surround the reservoir. In *N. lugens*, the reservoir expands upon dilator contraction, pumping saliva from the CSD through the salivarium and into the reservoir, which is likely the same mechanism for inflation of the salivarium employed in the insects examined here (Supporting Information: -Figure S5). The salivarium is connected distally to the ASD, which in turn is connected to the stylet fascicle. Relaxation of the dilator muscles would move saliva from the reservoir toward the ASD and the stylet fascicles.

4.4 | Interspecific disparities in scaling

Observed interspecific scale disparities in components of the feeding complex such as the cibarial dilator muscles, the food canal, and the precibarial canal likely translate to variation in fluid transport rates. The observed disparities of *X. fastidiosa* transmission efficiency between these vectors (Almeida, 2007; Almeida & Purcell, 2003; Cornara et al., 2016; Daugherty & Almeida, 2009) may be due to consequences of differences in size and structure of the feeding complex between these insect vectors; further study integrating muscle force application capabilities and fluid flow dynamics with these 3D morphological reconstructions will investigate this.

Dimensional measurements presented here were similar to other studies that have used SEM data (e.g., Almeida & Purcell, 2006; Rapicavoli et al., 2015) and 3D imaging data (Killiny & Brodersen, 2022; Ranieri et al., 2020) to visualize aspects of the sharpshooter feeding complex. The digital approach for measuring volume used here represents a promising tool in terms of speed and accuracy for calculating volume of critical areas of fluid flow and for calculating force application capabilities of the musculature. The method of preparation, although well-suited for visualizing insect soft tissue in 3D (Wood & Parkinson, 2019) can cause dehydration which may reduce the fidelity of the volume measurements of the samples (Metscher, 2009); alternative staining approaches may provide more accurate volume measurements (e.g., Swart et al., 2016). Nevertheless, the approach applied here represents the most high-resolution and accurate technique for measuring 3D volume of these anatomical features to date.

5 | CONCLUSIONS

Here, we applied synchrotron-based micro-CT imaging to visualize the feeding complex of three important xylem sap-feeding insect vectors of plant pathogens in 3D. We found that the volume of the cibarial dilator musculature in *H. vitripennis* was much larger compared to the other insects examined (e.g., over an order of magnitude larger than the cibarial dilator musculature of *G. atropunctata*), which indicates a dramatic difference in force application capabilities for fluid pumping between these insects. We found that the precibarial valve's flap closes completely, revealing an additional level of control over fluid flow in the feeding complex and a factor that may affect pathogen transmission. The attachment site of the precibarial valve muscle was found to differ from previous interpretations, which resulted in an updated description of the mechanism for how the precibarial valve functions. We were also able to identify organs involved in salivary production and transport. These findings illuminate important functional aspects of the feeding complex, demonstrating the power of 3D imaging, modeling, and volumetric measurement techniques for improving our understanding of these and other important insect vectors of plant pathogens. Future work can integrate the 3D anatomical models of the food canal and precibarial canal presented here into computational fluid dynamics simulations to analyze the influence of the disparate morphological features between insects identified here as well as illuminate how the full closure of the precibarial valve would impact the dynamics of sap flow and bacterial transmission.

AUTHOR CONTRIBUTIONS

Rodrigo P. P. Almeida and Andrew J. McElrone obtained funding for this project. Elizabeth G. Clark, Andrew J. McElrone, Craig R. Brodersen, and Dilworth Y. Parkinson performed the 3D imaging. Elizabeth G. Clark reconstructed the 3D data with Andrew J.

McElrone, Craig R. Brodersen, and Dilworth Y. Parkinson and interpreted the results with Daniele Cornara and Rodrigo P. P. Almeida. Elizabeth G. Clark drafted the manuscript with input from all authors.

ACKNOWLEDGMENTS

We would like to thank the members of the Almeida Lab, Marilyne Uzest (French National Institute for Agriculture, Food and Environment), Diane Ullman (University of California, Davis), Liz Mendoza (University of California, Irvine), and Fred Larabee (San Jose State University) for helpful discussions, as well as Rodrigo Krugner for providing *H. vitripennis* specimens for scanning. We would like to acknowledge beamline 8.3.2 of the Advanced Light Source along with the Advanced Light Source staff in the assistance of these experiments. This research was supported by an award from the California Department of Food and Agriculture PD/GWSS Research Program (CDFA Agreement Number 21-0274-000-SA). This research used resources of the Advanced Light Source, a US DOE Office of Science User Facility under contract no. DE-AC02-05CH11231. The participation of Daniele Cornara in this work was supported by a research grant in the frame of European Union's Horizon 2020 research and innovation program under the Marie Skłodowska-Curie grant agreement No 835732 XYL-SPIT.

CONFLICT OF INTEREST STATEMENT

The authors declare no conflict of interest.

DATA AVAILABILITY STATEMENT

The data that support the findings of this study are openly available in Dryad at https://doi.org/10.5061/dryad.s4mw6m99s.

PEER REVIEW

The peer review history for this article is available at https://www.webofscience.com/api/gateway/wos/peer-review/10.1002/jmor.21639.

REFERENCES

Alfaress, S., Brodersen, C. R., Ammar, E.-D., Rogers, M. E., & Killiny, N. (2018). Laser surgery reveals the biomechanical and chemical signaling functions of aphid siphunculi (cornicles). *PLoS One*, *13*, e0204984.

Almeida, R. P. P. (2007). Glassy-winged sharpshooter transmission of *Xylella fastidiosa* to plants. *Proceedings of the Hawaiian Entomological Society*, *39*, 83–86.

Almeida, R. P. P., & Purcell, A. H. (2003). Transmission of *Xylella fastidiosa* to grapevines by *Homalodisca coagulata* (Hemiptera: Cicadellidae). *Arthropods in Relation to Plant Diseases*, *96*, 264–271.

Almeida, R. P. P., & Purcell, A. H. (2006). Patterns of *Xylella fastidiosa* colonization of the precibarium of sharpshooter vectors relative to transmission to plants. *Arthropods in Relation to Plant Diseases*, *99*, 884–890.

Backus, E. A. (1985). Anatomical and sensory mechanisms of leafhopper and planthopper feeding behavior. In L. R. Nault & J. G. Rodriguez (Eds.), *The Leafhoppers and Planthoppers* (pp. 163–194).

Backus, E. A., Andrews, K. B., Shugart, H. J., Carl Greve, L., Labavitch, J. M., & Alhaddad, H. (2012). Salivary enzymes are injected into xylem by the glassy-winged sharpshooter, a vector of *Xylella fastidiosa*. *Journal of Insect Physiology*, *58*(7), 949–959.

Backus, E. A., & McLean, D. L. (1982). The sensory systems and feeding behavior of leafhoppers. I. The aster leafhopper, *Macrosteles fascifrons* Stål (Homoptera, Cicadellidae). *Journal of Morphology*, *172*, 361–379.

Bergman, E. A., Green, E. L., & Matthews, P. G. D. (2021). The cibarial pump of the xylem-feeding froghopper *Philaenus spumarius* produces negative pressures exceeding 1MPa. *Proceedings of the Royal Society B: Biological Sciences*, *288*, 20210731.

Chapman, R. F. (1998). *The insects: Structure and function*. Cambridge University Press.

Cignoni, P., Callieri, M., Corsini, M., Dellepiane, M., Ganovelli, F., & Ranzuglia, G. (2008). MeshLab: An open-source mesh processing tool. *In Sixth Eurographics Italian Chapter Conference*, 129–136.

Clark, E. G., Jenkins, K. M., & Brodersen, C. R. (2023). Back to life: Techniques for developing high-quality 3D reconstructions of plants and animals from digitized specimens. *PLoS One*, *18*, e0283027.

Cornara, D., Morente, M., Markheiser, A., Bodino, N., Tsai, C. W., Fereres, A., Redak, R. A., Perring, T. M., & Lopes, J. R. S. (2019). An overview on the worldwide vectors of *Xylella fastidiosa*. *Entomologia Generalis*, *39*(3/4), 157–181.

Cornara, D., Sicard, A., Zeilinger, A. R., Porcelli, F., Purcell, A. H., & Almeida, R. P. P. (2016). Transmission of *Xylella fastidiosato* grapevine by the meadow spittlebug. *Phytopathology*, *106*, 1285–1290.

Cryan, J. R., & Urban, J. M. (2012). Higher-level phylogeny of the insect order Hemiptera: Is auchenorrhynca really paraphyletic? *Systematic Entomology*, *37*, 7–21.

Daugherty, M. P., & Almeida, R. P. P. (2009). Estimating *Xylella fastidiosa* transmission parameters: Decoupling sharpshooter number and feeding period. *Entomologia Experimentalis et Applicata*, *132*, 84–92.

Gürsoy, D., De Carlo, F., Xiao, X., & Jacobsen, C. (2014). TomoPy: A framework for the analysis of synchrotron tomographic data. *Journal of Synchrotron Radiation*, *21*, 1188–1193.

Killiny, N., & Brodersen, C. R. (2022). Using X-ray micro-computed tomography to three-dimensionally visualize the foregut of the glassy-winged sharpshooter (*Homalodisca vitripennis*). *Insects*, *13*, 710.

Krugner, R., & Gordon, S. D. (2018). Mating disruption of *Homalodisca vitripennis* (Germar) (Hemiptera: Cicadellidae) by playback of vibrational signals in vineyard trellis. *Pest Management Science*, *74*, 2013–2019.

Leopold, R. A., Freeman, T. P., Buckner, J. S., & Nelson, D. R. (2003). Mouthpart morphology and stylet penetration of host plants by the glassy-winged sharpshooter, *Homalodisca coagulata*, (Homoptera: Cicadellidae). *Arthropod Structure & Development*, *32*, 189–199.

Metscher, B. D. (2009). MicroCT for developmental biology: A versatile tool for high-contrast 3D imaging at histological resolutions. *Developmental Dynamics*, *238*, 632–640.

Mittler, T. E. (1967). Water tensions in plants—An entomological approach1. *Annals of the Entomological Society of America*, *60*, 1074–1076.

Nault, L. R., & Ammar, E. D. (1989). Leafhopper and planthopper transmission of plant viruses. *Annual Review of Entomology*, *34*, 503–529.

Purcell, A. H. (1979). Evidence for noncirculative transmission of Pierce's disease bacterium by sharpshooter leafhoppers. *Phytopathology*, *69*, 393–395.

Purcell, A. H., & Saunders, S. R. (1999). Glassy-winged sharpshooters expected to increase plant disease. *California Agriculture*, *53*, 26–27.

Ranieri, E., Zitti, G., Riolo, P., Isidoro, N., Ruschioni, S., Brocchini, M., & Almeida, R. P. P. (2020). Fluid dynamics in the functional foregut of xylem sap-feeding insects: A comparative study of two *Xylella fastidiosa* vectors. *Journal of Insect Physiology*, *120*, 103995.

Rapicavoli, J. N., Kinsinger, N., Perring, T. M., Backus, E. A., Shugart, H. J., Walker, S., & Roper, M. C. (2015). O antigen modulates insect vector

acquisition of the bacterial plant pathogen *Xylella fastidiosa*. *Applied and Environmental Microbiology*, *81*, 8145–8154.

Raven, J. A. (1983). Phytophages of xylem and phloem: A comparison of animal and plant sap-feeders, *Advances in ecological research* (vol.13, pp. 135–234). Academic Press.

Redak, R. A., Purcell, A. H., Lopes, J. R. S., Blua, M. J., Mizell, III, R. F., & Andersen, P. C. (2004). The biology of xylem fluid-feeding insect vectors of *Xylella fastidiosa* and their relation to disease epidemiology. *Annual Review of Entomology*, *49*, 243–270.

Ruschioni, S., Ranieri, E., Riolo, P., Romani, R., Almeida, R. P. P., & Isidoro, N. (2019). Functional anatomy of the precibarial valve in *Philaenus spumarius* (L.). *PLoS One*, *14*, e0213318.

Sicard, A., Zeilinger, A. R., Vanhove, M., Schartel, T. E., Beal, D. J., Daugherty, M. P., & Almeida, R. P. P. (2018). *Xylella fastidiosa*: Insights into an emerging plant pathogen. *Annual Review of Phytopathology*, *56*, 181–202.

Snodgrass. (1935). *Principles of insect morphology*. McGraw-Hill Book Co.

Swart, P., Wicklein, M., Sykes, D., Ahmed, F., & Krapp, H. G. (2016). A quantitative comparison of micro-CT preparations in Dipteran flies. *Scientific Reports*, *6*, 39380.

Tumber, K. P., Alston, J. M., & Fuller, K. B. (2014). Pierce's disease costs California $104 million per year. *California Agriculture*, *68*, 20–29.

Wang, X.-Q., Guo, J., Li, D.-T., Yu, Y., Hagoort, J., Moussian, B., & Zhang, C.-X. (2021). Three-dimensional reconstruction of a whole insect reveals its phloem sap-sucking mechanism at nano-resolution. *eLife*, *10*, e62875.

White, D., Backus, E. A., Marcus, I. M., Walker, S. L., & Roper, M. C. (2021). Functional foregut anatomy of the blue-green sharpshooter illustrated using a 3D model. *Scientific Reports*, *11*, 6536.

Wood, H. M., & Parkinson, D. Y. (2019). Comparative morphology of cheliceral muscles using high-resolution X-ray microcomputed-tomography in palpimanoid spiders (Araneae, Palpimanoidea). *Journal of Morphology*, *280*, 232–243.

SUPPORTING INFORMATION

Additional supporting information can be found online in the Supporting Information section at the end of this article.

How to cite this article: Clark, E. G., Cornara, D., Brodersen, C. R., McElrone, A. J., Parkinson, D. Y., & Almeida, R. P. P. (2023). Anatomy of an agricultural antagonist: Feeding complex structure and function of three xylem sap-feeding insects illuminated with synchrotron-based 3D imaging. *Journal of Morphology*, *284*, e21639. https://doi.org/10.1002/jmor.21639